Frequency-Dependent Fluidic Inductance and Resistance in Inkjet Passages

Douglas D. Darling
Xerox Corporation
Wilsonville, Oregon, USA

Abstract

Accurate analysis of the dynamic response of an inkjet is important to compare various geometries and predict the effect of potential design changes. The fluid in an inkjet typically has a low Reynolds number (i.e. viscous forces are important) and often oscillates quickly (relative to the timescale of boundary layer to development). It is well known that, when a viscous flow oscillates, the shape of the velocity profile is dependent on the passage geometry and the frequency of the oscillation. The viscous boundary layer effectively blocks part of the cross-section of the passage, changing the required pressure to accelerate (inductance) and sustain (resistance) the flow. Thus, the fluidic resistance and inductance are functions of both geometry and frequency. The resistance is least at low frequencies and increases with frequency. Inductance is highest at low frequency and decreases with frequency. The effect of inductance on impedance still increases with frequency. An analytical correlation for fluidic inductance and resistance has been developed. Frequency dependent inductance and resistance were important to accurately predict the resonant frequencies and the extent of damping in an inkjet.

Nomenclature

a,b	height and width of rectangular passage
c	speed of sound
C	fluidic capacitance, based on mass flow
D	diameter of circular passage
f	frequency of oscillation
L	fluidic inductance, based on mass flow
$\dot{m}$	mass flow rate, integrated across flow area
p	fluid pressure
r	radial dimension
R	fluidic resistance, based on mass flow
Rad	overall radius of circular passage (D/2)
t	time
u	velocity in the primary flow direction (z)
x, y	dimensions across rectangular passage
z	primary flow direction
μ	fluid viscosity
ρ	fluid density
ω	$2\pi f$

Introduction

Accurate analysis of the dynamic response of an inkjet is important to compare various geometries and predict the effect of potential design changes. One possibility is CFD. A full CFD analysis of the inkjet can yield a good understanding of the detailed fluid dynamics of an inkjet. However, CFD is often too time consuming for parametric studies, or quick analysis during problem solving. In those cases, it is good to have a simplified model, such as discussed in this paper. In simplified models, an inkjet is typically treated as an acoustic circuit. The fluid passages are divided into fluidic inductors (L), capacitors (C) and resistors (R) (see Reference 1, for example). Unsteady analysis is performed using the integrated mass flow across the passage, along with the L, C and R, calculated based on the geometry of the passage and the fluid properties.

It is well known that the velocity profile changes if the frequency of the pressure gradient changes (References 2 and 3). Changes in the velocity profile will affect a couple things: (1) The shear stresses at the walls change, and therefore the fluidic resistance, R, changes. (2) The momentum displacement of the boundary layer changes. That affects how much inertia is associated with a given integrated mass flow; therefore the fluidic inductance, L, changes. In this work we will quantify how the variations in the velocity profile affect the inductance and resistance, used to model an inkjet.

Analysis

Figure 1 shows a sketch of a typical inkjet. The inlet connects the inkjet with the manifold. The body has a diaphragm and PZT on one side; which drives the inkjet. The outlet allows ink to flow between the body chamber and the aperture, where drops are ejected.

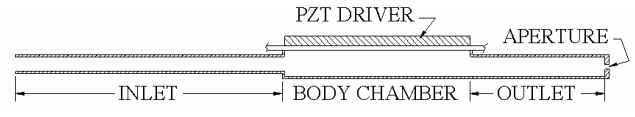

Figure 1. Sketch of PZT-driven inkjet

The following are the assumptions used in the analysis:

1. The Reynolds Number (Re) is low (<1). This means that the flow is laminar, and that we can neglect the non-linear pressure drop ($\propto \rho * u^2$) terms.
2. The cross section is very small relative to a wavelength of sound. Pressure and density are then effectively constant across the passage, and are treated as functions of the primary flow dimension (z) and time (t).
3. Perturbations in density are small relative to the mean density. The mean density is then used in the momentum equation, and compressibility is restricted to the continuity equation. This is a common assumption in acoustics (Reference 4).
4. $\frac{\partial u}{\partial t} >> u\frac{\partial u}{\partial z}$.

   This can be true due to a couple of reasons. (1) First, the assumption is true if the Mach Number is small (this is needed, because the flow is compressible in the z-direction) AND the entrance length is short relative to the length of the passage (good for small Re and long lengths) AND there are no variations in flow area occurring on length scale of a wavelength. This is how this assumption is made in fluid mechanics references (e.g. Reference 2). In this paper, the fluid passages are treated as constant area sections. Discrete area changes are treated by acoustic relationships (References 3 and 4). (2) This assumption is also true if the f*D/u is large, either because the frequency (or geometry) is large or the velocity is low. This is how acoustics references can make this assumption (e.g. Reference 4).
5. The motion of the meniscus is small relative to the size of the aperture. Thus, the inductance and resistance of the aperture are treated as constant in time, and the model is linear. This is not true when a drop is being ejected, but was true when the impedance of the inkjet was measured to compare with this analysis. The analysis of the other fluid passages would be valid without this assumption.
6. The inkjet has reached its steady-state response (i.e. it is a frequency-domain analysis, not time-domain).

Circular Passages

Circular passages will be considered first, followed by rectangular passages. Using the assumptions above, the z-momentum equation becomes Equation 1:

$$\rho\frac{\partial u}{\partial t} = -\frac{\partial p}{\partial z} + \frac{\mu}{r}\frac{\partial}{\partial r}\left(r\frac{\partial u}{\partial r}\right) \tag{1}$$

The solution variables, p and u, are split into functions of z, r, and t:

$$u = \tilde{u}(z)\hat{u}(r)e^{i\omega t}, \qquad \frac{\partial p}{\partial z} = \tilde{K}(z)e^{i\omega t} \tag{2}$$

Then, the momentum equation becomes Equation 3.

$$i\rho\omega\,\hat{u} = -K + \frac{\mu}{r}\frac{\partial}{\partial r}\left(r\frac{\partial \hat{u}}{\partial r}\right) \tag{3}$$

where

$$K = \tilde{K}(z)/\tilde{u}(z).$$

The solution to Equation 3 is given in Reference 2:

$$\hat{u}(r) = \frac{iK}{\rho\omega}\left\{1 - \frac{J_0\left(r\sqrt{\frac{-i\rho\omega}{\mu}}\right)}{J_0\left(Rad\sqrt{\frac{-i\rho\omega}{\mu}}\right)}\right\} \tag{4}$$

(The definition of "K" in Equation 4 is not quite the same as in the reference.)

Equation 4 is closed form, and can be easily analyzed and integrated to determine the fluidic inductance and resistance, relative to the average mass flow rate in the passage. The result is, of course, frequency dependent.

Figure 2 gives the velocity profiles for a cycle at a relatively low frequency. At this relatively low frequency, the velocity profile is close to the parabolic, steady-state shape. And, the velocity is close to being in phase with the negative of the pressure gradient. The fluidic resistance and inductance per unit length are close to values for a steady-state velocity profile.

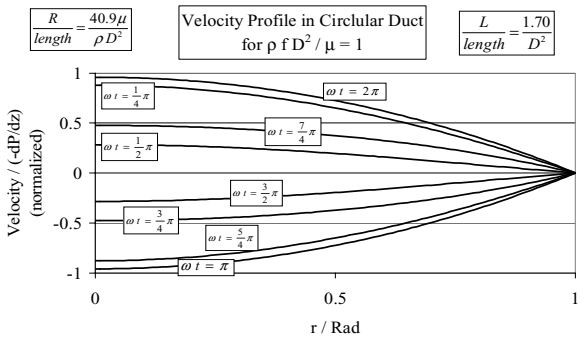

Figure 2. Velocity profiles in a circular passage at low frequency.

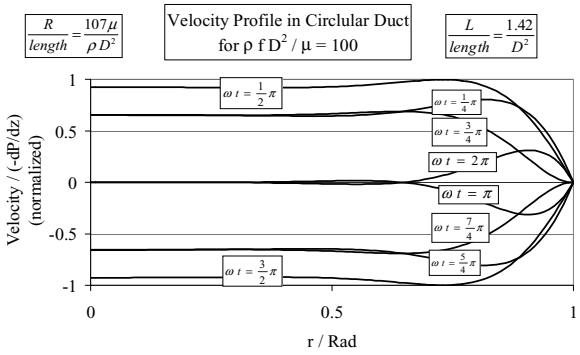

Figure 3. Velocity profiles in a circular duct for high frequency.

At higher frequencies the velocity profile has a different character. As shown in Figure 3, the velocity profile is flatter near the centerline of the passage, than was the low frequency case. The velocity at the centerline lags the negative of the pressure gradient by about π/2rad. The fluidic resistance and inductance, per unit length, are now significantly different than the low-frequency limit.

To avoid solving Equation 4 for every frequency every time an analysis is performed, a similarity analysis was performed. From the equations above, the obvious independent similarity variable is the following.

$$X_1 \equiv \frac{\rho f D^2}{\mu} \tag{5}$$

The dependent similarity variables were chosen to be relative to the minimum resistance and minimum inductance:

$$Y_1 \equiv \frac{R}{R_{\min}} \quad Y_2 \equiv \frac{L}{L_{\min}} \tag{6}$$

The minimum resistance occurs at the low frequency limit, and is given by Equation 7.

$$\frac{R_{\min}}{length} = \frac{128\mu}{\pi\rho D^4} \approx \frac{40.7\mu}{\rho D^4} \tag{7}$$

The minimum inductance occurs at the high frequency limit, and is given by the following.

$$\frac{L_{\min}}{length} = \frac{1}{Area} = \frac{4}{\pi D^2} \tag{8}$$

Y_1 and Y_2 are unique functions of X_1 (see Figure 4). Note that the resistance can vary by several times. The resistance increases as the velocity gradient at the wall increases with frequency. Meanwhile, the inductance varies by 33% from its minimum value. The inductance decreases as the velocity profile becomes flatter, as the frequency increases. In order to perform a frequency domain analysis, one can simply calculate the minimum resistance and inductance, and then use the values shown in Figure 4 as a correction factor at each frequency. The results can be used by a table lookup or a curve fit. Equations 9 and 10 are suggested curve fits for the functions in Figure 4.

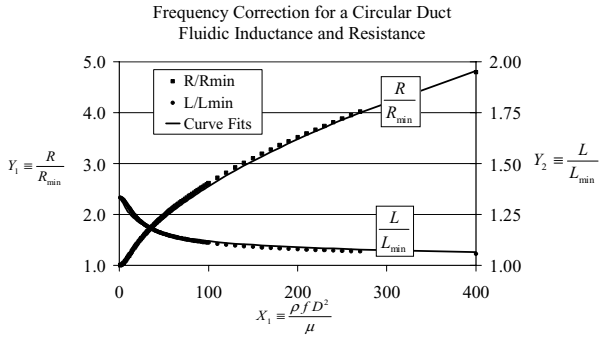

Figure 4. Frequency corrections for a circular passage

$$Y_1 \equiv \frac{R}{R_{min}} \approx (0.009882)\left(e^{-0.756X_1} + 23.93\right)\sqrt{X_1 + 16.48} \tag{9}$$

$$Y_2 \equiv \frac{L}{L_{\min}} \approx \frac{(X_1 + 3.27)^{0.807}}{(X_1 + 5.11)^{1.26}} + 1 \tag{10}$$

Rectangular Passages

Of course, not all of the passages in an inkjet are have circular cross sections. A similar analysis can be performed for a rectangular passage (Figure 5). The lengths of the sides of the rectangular passage are b and a, where b is greater than or equal to a. Thus, b/a is greater than or equal to 1.

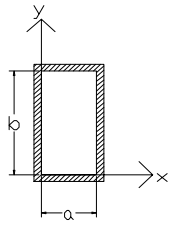

Figure 5. Rectangular passage (b>a).

We will not go through all of the details here, since it is essentially the same process as above. Using the same assumptions as for the circular passage, the oscillating velocity profile of a rectangular passage the can be expressed as the following:

$$\hat{u}(x,y) = -\frac{16K}{\pi^2} \sum_{m=1,3,5,\ldots}^{\infty} \sum_{n=1,3,5,\ldots}^{\infty} \frac{\sin\left(\frac{m\pi x}{a}\right)\sin\left(\frac{n\pi y}{b}\right)}{\left[\pi^2\mu\left(\frac{m^2}{a^2}+\frac{n^2}{b^2}\right)+i\rho\omega\right]mn} \tag{11}$$

Figure 6 shows the sequence of velocity profiles over one cycle, relative to the negative of the pressure gradient. The case shown is for a square passage (a=b) at a moderate frequency. The frequency is high enough that the velocity at the center of the passage lags the negative pressure gradient by about π/2rad, but it is not high enough to make the profile particularly flat. A higher frequency would result in a flatter profile; a lower frequency would result in a velocity in phase with the negative pressure gradient.

The velocity profile equation can be integrated and the result can be expressed as the fluidic impedance per unit length (Equation 12):

$$\frac{Z}{length} = \frac{\left(\frac{\pi^4}{64\rho ab}\right)}{\sum_{m=1,3,5,\ldots}^{\infty} \sum_{n=1,3,5,\ldots}^{\infty} \frac{1}{\left[\pi^2\mu\left(\frac{m^2}{a^2}+\frac{n^2}{b^2}\right)+i\rho\omega\right]m^2n^2}} \tag{12}$$

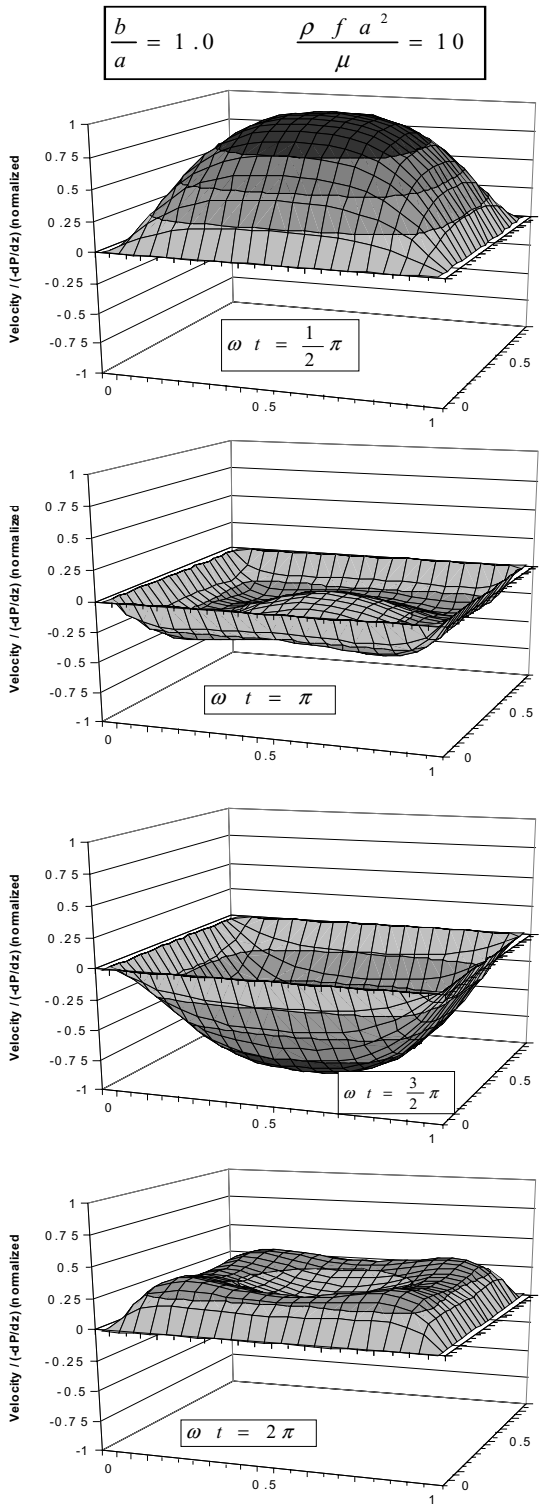

Figure 6. Velocity profiles for a square passage at a moderate frequency

Note, Equation 12 only includes resistance and inductance. Recall, from Assumptions 2 and 3, the compressibility is treated only in the flow (z) direction, so will not appear in this expression. The fluidic capacitance will still be expressed as in standard acoustic transmission line models:

$$\frac{C}{length}\cdot\frac{\partial p(z,t)}{\partial t}=-\frac{\partial \dot{m}(z,t)}{\partial z} \tag{13}$$

$$\frac{C}{length}=\frac{Area}{c^2}=\frac{ab}{c^2} \tag{14}$$

Equation 12 can be spilt into real and imaginary parts, to separate the resistance and inductance.

$$\frac{R}{length}=\left(\frac{\mu\pi^6}{64\rho ab}\right)\frac{\sum_m\sum_n\frac{\left(\frac{m^2}{a^2}+\frac{n^2}{b^2}\right)}{\pi^4\mu^2m^2n^2\left(\frac{m^2}{a^2}+\frac{n^2}{b^2}\right)^2+\rho^2\omega^2m^2n^2}}{\left(\sum_m\sum_n\frac{\pi^2\mu\left(\frac{m^2}{a^2}+\frac{n^2}{b^2}\right)}{\pi^4\mu^2m^2n^2\left(\frac{m^2}{a^2}+\frac{n^2}{b^2}\right)^2+\rho^2\omega^2m^2n^2}\right)^2+\left(\sum_m\sum_n\frac{\rho\omega}{\pi^4\mu^2m^2n^2\left(\frac{m^2}{a^2}+\frac{n^2}{b^2}\right)^2+\rho^2\omega^2m^2n^2}\right)^2}$$

$$for\ m=1,3,5,7,9,\ldots\infty\quad\&\quad n=1,3,5,7,9,\ldots\infty \tag{15}$$

$$\frac{L}{length}=\left(\frac{\pi^4}{64ab}\right)\frac{\sum_m\sum_n\frac{1}{\pi^4\mu^2m^2n^2\left(\frac{m^2}{a^2}+\frac{n^2}{b^2}\right)^2+\rho^2\omega^2m^2n^2}}{\left(\sum_m\sum_n\frac{\pi^2\mu\left(\frac{m^2}{a^2}+\frac{n^2}{b^2}\right)}{\pi^4\mu^2m^2n^2\left(\frac{m^2}{a^2}+\frac{n^2}{b^2}\right)^2+\rho^2\omega^2m^2n^2}\right)^2+\left(\sum_m\sum_n\frac{\rho\omega}{\pi^4\mu^2m^2n^2\left(\frac{m^2}{a^2}+\frac{n^2}{b^2}\right)^2+\rho^2\omega^2m^2n^2}\right)^2}$$

$$for\ m=1,3,5,7,9,\ldots\infty\quad\&\quad n=1,3,5,7,9,\ldots\infty \tag{16}$$

Equations 15 and 16 are cumbersome, to say the least. So, a similarity analysis was performed again. This time, there were two independent similarity variables:

$$X_1\equiv\frac{\rho f a^2}{\mu},\quad X_2\equiv\frac{b}{a} \tag{17}$$

The dependent similarity variables are the same as for a circular passage.

$$Y_1\equiv\frac{R}{R_{\min}}\quad Y_2\equiv\frac{L}{L_{\min}} \tag{18}$$

The minimum resistance still occurs at the low frequency limit and is given by Equation 19 (Reference 3).

$$\frac{R_{\min}}{length}=\frac{\left(\frac{12\mu}{\rho ba^3}\right)}{1-\frac{192a}{\pi^5 b}\sum_{m=1,3,5,\ldots}^{\infty}\frac{\tanh\left(\frac{m\pi b}{2a}\right)}{m^5}} \tag{19}$$

This expression will work whether b<a or a>b, but the series will converge much faster if the variables are defined such that b>a. The minimum inductance still occurs at the high frequency limit. It is given by Equation 20.

$$\frac{L_{\min}}{length} = \frac{1}{Area} = \frac{1}{ab} \tag{20}$$

The relationships between the similarity variables are given on Figures 7, 8, 9 and 10. Again, these values can be used to correct the inductance and resistance for a frequency domain calculation.

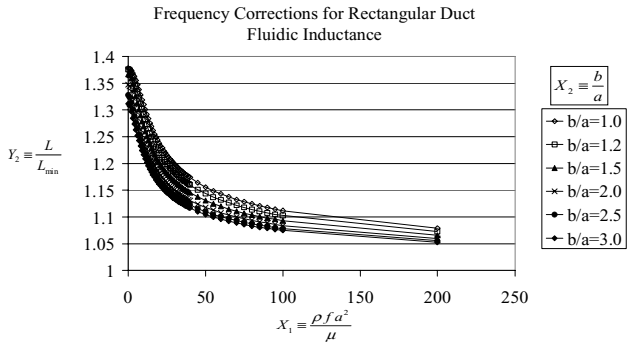

Figure 7. Inductance correction for a rectangular passage for b/a from 1.0 to 3.0

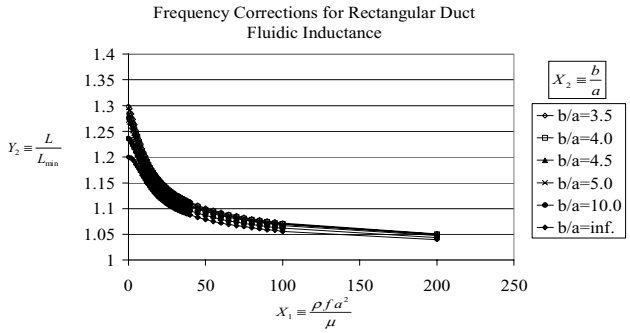

Figure 8. Inductance correction for a rectangular passage for b/a from 3.5 to infinity.

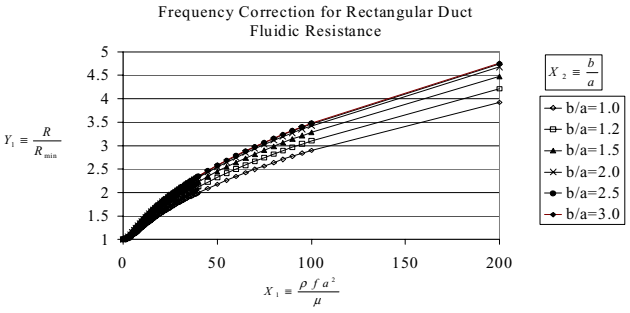

Figure 9. Resistance correction for a rectangular passage for b/a from 1.0 to 3.5

Generally, the trends are the same as for the circular profile. The resistance can vary by several times, as the wall shear stress varies with frequency. The frequency correction for resistance is not monotonic with aspect ratio. The correction for R is at its maximum for b/a of about 3.1. However, that does not mean the actual resistance is at its maximum for b/a of 3.1, since a and b are also in the expression for R_{min}. For a given cross-sectional area, the maximum resistance occurs as b/a→∞. The fluidic inductance is at its maximum as frequency approaches zero. The correction for inductance is monotonic with aspect ratio. At the low frequency limit, the correction varies from 1.20 for a slot (b/a→∞) to 1.38 for a square (b/a=1). As the frequency approaches infinity, the correction for inductance approaches unity for all aspect ratios.

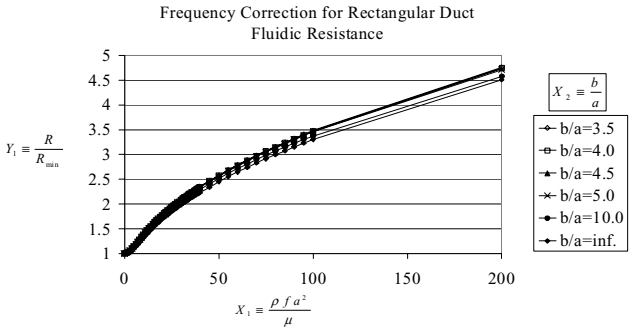

Figure 10. Resistance correction for a rectangular passage for b/a from 3.5 to infinity

Finally, these frequency corrections were made to the frequency domain analysis of an inkjet. The remainder of the analysis is as described in Ref. 1: acoustic transmission lines, linear perturbations. The extra impedance associated with sudden changes in area, were analyzed using expressions from Refs. 4 and 5.

Validation

The Xerox Phaser8400 inkjet was analyzed. The results were compared with measurements made using an impedance analyzer. An electrical signal was applied to the PZT driver, and the real part of the admittance was recorded. The real part of the admittance was chosen, because it was indicative of the energy being absorbed by the inkjet. During these measurements, the applied voltage was much smaller than would be required to eject a drop. Thus, the meniscus moved little compared with drop ejection. So, the inductance and resistance of the aperture were sufficiently constant in time that the linear assumption was valid.

Figure 11 shows a typical measured admittance sweep. The general upward slope of the curve was due to the electrical components; it was the tail end of the much higher frequency mode of the electrical system. F_0 was the bulk fluid mode of the inkjet, where the body and outlet acted as a fluidic capacitor, while the inlet and aperture acted as fluidic resistors and inductors. It was highly damped, and it was difficult to observe above the measurement noise. The resolution of F_0 could have been be improved by increasing

the averaging and delay time of the instrument, but it was still much harder to see than either F_1 or F_2. F_1 was the first standing mode, involving (predominantly) the combined outlet and body chamber. It was much less damped than F_0, and could easily be seen above the measurement noise. F_2 was a standing wave involving (predominantly) the combined inlet and body chamber. It was more damped than F_1, but still much less damped than F_0. Of the three, F_1 could be measured with the least uncertainty, so it was used to compare with the analytical model.

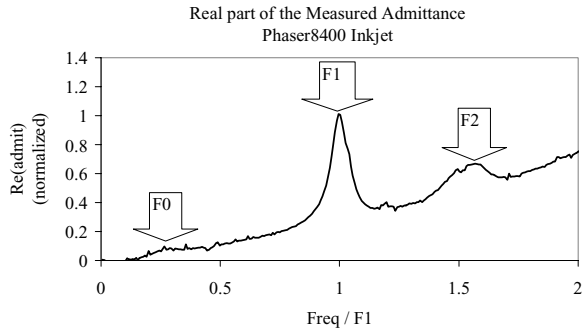

Figure 11. Typical admittance measurement of Phaser8400 inkjet.

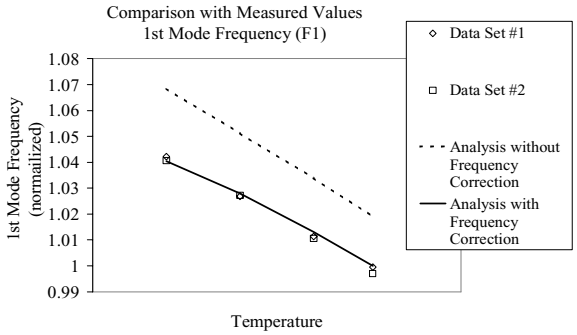

Figure 12. Comparison of analysis with experiment

The first standing mode frequency, F_1, was measured at four temperatures. And, the test was repeated using different hardware. Then, the value for F_1 was predicted, using the frequency-dependent analysis described above. The analysis was performed with and without the frequency corrections. Figure 12 shows both measured and predicted values for F_1, as the temperature of the inkjet was varied. Without the frequency correction for R and L, the analysis over-predicted F_1. When R and L were corrected for variations in the velocity profile, the agreement between the model and the experiment was improved.

Conclusion

Corrections were made to the fluidic inductance and resistance as a function of frequency, for analysis of inkjet passages. This was done to compensate for variations in the velocity profile. The corrections were made for inkjet passages with both circular and rectangular cross-sections. The frequency correction was expressed in terms of similarity variables, for easy application to frequency domain analyses. Without the correction, the error in fluidic resistance can be a factor of several times. The potential error in the fluidic inductance is more modest. For a circular passage, the fluidic inductance at the low frequency limit is 33% higher than at the high frequency limit. For a slot the fluidic inductance at the low frequency limit is 20% higher than at the high frequency limit. A square gives about 38%. Errors in the inductance and resistance have a direct effect on the predicted dynamic response of an inkjet.

References

1. S. S. Berger and G. Recktenwald, Development of an Improved Model for Piezo-Electric Driven Ink Jets, Proc. IS&T NIP19, pg 323-327. (2003)
2. H. Schlichting, Boundary Layer Theory, 7th Ed., McGraw-Hill Inc., 1979, pg. 436-438.
3. F. M. White, Viscous Fluid Flow, 2nd Ed., Mc-Graw-Hill Inc., 1991, pg. 116, 120, 135-136.
4. L. E. Kinsler, A. R. Frey, A. B. Coppens, J. V. Sanders, Fundamentals of Acoustics, 3rd Ed., John Wiley and Sons, 1982, pg. 104-105, 232-233.
5. P. M. Morse, K. U. Ingard, Theoretical Acoustics, Princeton University Press and McGraw-Hill Inc, 1986, pg. 472-484, 901.

Biography

Douglas Darling received a B.S. in Mechanical Engineering in 1986. Then, he earned his Ph.D. in Mechanical Engineering from the University of Illinois at Urbana-Champaign in 1989. Subsequently, he worked at NASA-Lewis Research Center (currently NASA-Glenn) and Siemens-Westinghouse Power Corporation on unsteady fluid dynamics and acoustics. Since 2000, he has worked at the Xerox Corporation in Wilsonville, Oregon, in solid ink printhead development.